2024 American Control Conference (ACC)
July 8-12, 2024. Toronto, Canada

Retrospective Cost-based Extremum Seeking Control with Vanishing Perturbation for Online Output Minimization

Juan A. Paredes, Jhon Manuel Portella Delgado, Dennis S. Bernstein, and Ankit Goel

Abstract— **Extremum-seeking control (ESC) is a powerful technique for online optimization that offers theoretical guarantees for convergence to the optimizer's neighborhood under well-understood conditions. However, ESC requires a nonconstant perturbation signal to provide persistent excitation to the target system to yield convergent results, which usually results in steady state oscillations. While certain techniques have been proposed to eliminate perturbations once the neighborhood of the minimizer is reached, system modifications and environmental perturbations can suddenly change the minimizer, and nonconstant perturbations would once more be required to converge to the new minimizer. Hence, this paper develops a retrospective cost-based ESC (RC/ESC) technique for online output minimization with a vanishing perturbation, that is, a perturbation that becomes zero as time increases independently from the state of the controller or the controlled system. The performance of the proposed algorithm is illustrated via numerical examples.**

I. Introduction

Extremum seeking control (ESC) is a powerful adaptive control technique that leverages persistent system excitation to search for extrema in order to either minimize or maximize a user-defined metric [1]. The stability and convergence properties of ESC and their conditions have been thoroughly studied and are well understood [2]–[4]. ESC has been applied in a wide arrange of fields, including robotics [5]–[8] and energy management [9]–[12].

A feature of ESC is a persistent perturbation signal, which enables gradient estimation algorithms to yield a search direction that points towards local extrema, thus enabling convergence. However, implementing this perturbation signal results in steady-state oscillations, which may be prohibitive in physical testing. Modifications to the ESC algorithm have been proposed to address this issue, which include modifying the perturbation signal to vanish depending on controller and system values and implementing dynamics that suppress the perturbation signal once a neighborhood of the minimizer has been reached [13]–[17].

The contribution of this paper is thus an ESC algorithm for online output minimization with a vanishing perturbation, that is, a perturbation that becomes zero as time increases independently from the state of the controller or the controlled system. Hence, the perturbation is independent from the rest of the system and no extra dynamics are required to suppress the perturbation. In particular, we consider retrospective cost adaptive control (RCAC), which re-optimizes the coefficients of the feedback controller at each step [18]. A similar retrospective cost algorithm was proposed in [19], [20], in which a fixed target model was used to issue a search direction in the input space for optimization. In this work, a Kalman Filter (KF) is used to estimate the gradient of the system output which is encoded into the target model to provide a time-varying search direction to RCAC. Hence, the combination of the KF, the target model construction procedure, and RCAC yields retrospective cost based ESC (RC/ESC). A preliminary version of this algorithm was considered in [21], in which gradient estimation was performed by using a simple high-pass filter. Furthermore, the present work constitutes an extension of the algorithm considered in [22] by allowing the RCAC controller to have either an autoregressive-moving-average (ARMA) or PID-based structure and not requiring an initialization period for the KF.

The contents of the paper are as follows. Section II provides a statement of the control problem, which involves continuous-time dynamics under sampled-data feedback control. Section III provides a review of continuous-time ESC. Section IV introduces RC/ESC, in which a KF estimates the gradient of the system output and provides a target model to RCAC. Section V presents numerical examples that illustrate the performance of RC/ESC, including examples with static maps and a example with a dynamic system. Finally, VI presents conclusions.

Notation: $\mathbf{q} \in \mathbb{C}$ denotes the forward-shift operator.

II. Problem Statement

We consider continuous-time dynamics under sampled-data control using discrete-time adaptive controllers to reflect the practical implementation of digital controllers for physical systems. In particular, we consider the control architecture shown in Figure 1, where $\mathcal{M}$ is the target continuous-time system, $t \geq 0$, $u(t) \in \mathbb{R}^m$ is the control, and $J(t) \in \mathbb{R}^p$ is the output of $\mathcal{M}$, whose components are all nonnegative; the nonnegativity of the components of J is chosen to better accommodate output minimization problems that appear in control applications, such as steady-state error and nonlinear oscillation minimization.

The output $J(t)$ is sampled to generate the measurement $J_k \in \mathbb{R}^p$, which, for all $k \geq 0$, is given by

$$J_k \overset{\triangle}{=} J(kT_{\rm s}), \tag{1}$$

where $T_{\rm s} > 0$ is the sample time. The adaptive controller, which is updated at each step k, is denoted by $\mathcal{G}_{{\rm c},k}$. The input to $\mathcal{G}_{{\rm c},k}$ is J_k, and its output at each step k is the discrete-time control $u_k \in \mathbb{R}^m$. The continuous-time control signal

Juan A. Paredes and Dennis S. Bernstein are with the Department of Aerospace Engineering, University of Michigan, Ann Arbor, MI, USA. {jparedes, dsbaero}@umich.edu

Jhon Manuel Portella and Ankit Goel are with the Department of Mechanical Engineering, University of Maryland, Baltimore County, MD 21250. {jportella,ankgoel}@umbc.edu

979-8-3503-8264-8/$31.00 ©2024 AACC

$u(t)$ applied to the structure is generated by applying a zero-order-hold operation to u_k, that is, for all $k \geq 0$, and, for all $t \in [kT_{\rm s}, (k+1)T_{\rm s})$,

$$u(t) = u_k. \tag{2}$$

The objective of the adaptive controller is to yield an input signal that minimizes the output of the continuous-time system, that is, yield $u(t)$ such that $\lim_{t\to\infty} J(t) = 0$.

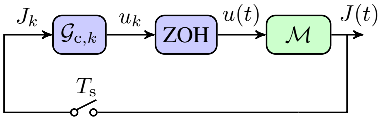

Fig. 1: Sampled-data implementation of adaptive controller for control of the continuous-time system $\mathcal{M}$. All sample-and-hold operations are synchronous. The adaptive controller uses J_k as an input and generates the discrete-time control u_k at each step k. Note that all components of J_k are nonnegative. The resulting continuous-time control $u(t)$ is generated by applying a zero-order-hold operation to u_k. The objective of the controller is to yield an input signal that minimizes the output of the continuous-time system, that is, yield $u(t)$ such that $\lim_{t\to\infty} J(t) = 0$.

III. Overview of Extremum Seeking Control

A. General Scheme

Consider the system $\mathcal{M}$ shown in first-order extremum seeking scheme displayed in figure 2 to be

$$\dot{x} = f(x,u), \tag{3}$$
$$J(t) = \mathcal{Q}(x), \tag{4}$$

where $f : \mathbb{R}^n \times \mathbb{R}^m \to \mathbb{R}^n$ and $\mathcal{Q}(x) : \mathbb{R}^n \to \mathbb{R}^p$ are smooth enough, $x \in \mathbb{R}^n$ is the measured vector state, $u \in \mathbb{R}^m$ is the input vector and $J(t) \in \mathbb{R}^p$ is the output of the cost function $\mathcal{Q}(x)$. Suppose that there exists x^* such that $J^* = \mathcal{Q}(x^*)$ is the extremum of the map $\mathcal{Q}(.)$. Assume that both x^* and $\mathcal{Q}(.)$ are unknown. Thus, the main goal of extremum seeking control is to drive the states of the closed loop to x^* without knowledge of x^* or $\mathcal{Q}(.)$

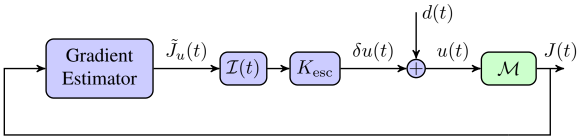

Fig. 2: Continuous-time extremum seeking control (ESC) of the continuous-time system $\mathcal{M}$. ESC uses J as an input and generates the control u_k at each step k. Note that all components of J are nonnegative. The objective of the controller is yield an input signal that minimizes the output of the continuous-time system, that is, yield $u(t)$ such that $\lim_{t\to\infty} J(t) = 0$.

B. SISO case

Consider the case when $J(x) \in \mathbb{R}$, and $u \in \mathbb{R}$ are scalar. Next, consider the dither signal

$$d(t) = a\ \sin(\omega_1\ t), \tag{5}$$

where a is the amplitude of the dither signal, and ω_1 is the dither frequency. Also, note that the gradient estimator used in this work is based on the averaging technique as proven in [23], such that

$$\tilde{J}_u(t) = \frac{2}{a}\ J(t)\sin(\omega_1\ t). \tag{6}$$

Finally, $\delta u(t)$, computed as the output of $\mathcal{I}(t)$ shown in figure 2, is obtained from the gradient-descent scheme given by

$$\delta u(t) = K_{\rm esc} \int_0^t \tilde{J}_u\ dt. \tag{7}$$

In this scheme, a, ω_1 and $K_{\rm esc}$ are the tuning parameters.

C. MISO case

Now, consider the case when $J(x) \in \mathbb{R}$, and $u \in \mathbb{R}^m$. Define the vector of dither signals $\mathcal{D}(t) \triangleq \begin{bmatrix} d_1(t) & d_2(t) & \cdots & d_m(t)\end{bmatrix}^{\rm T}$ given by

$$\mathcal{D}(t) = a \begin{bmatrix}\sin(\omega_1\ t) & \sin(\omega_2\ t) & \ldots & \sin(\omega_m\ t)\end{bmatrix}^{\rm T}, \tag{8}$$

where each $\omega_1, \omega_2, \cdots, \omega_m$ must be different. Note that although different amplitudes can be chosen for each dither signal, in the present work the same amplitude has been used for all, as shown in (8). Define $\tilde{\mathcal{J}}_u \triangleq \begin{bmatrix}\tilde{J}_{u_1} & \tilde{J}_{u_2} & \cdots & \tilde{J}_{u_m}\end{bmatrix}^{\rm T}$. Then, the gradient estimator based on the work done by [24] is given by

$$\tilde{\mathcal{J}}_u = \frac{2}{a}\ J(t) \begin{bmatrix}\sin(\omega_1\ t) & \sin(\omega_2\ t) & \ldots & \sin(\omega_m\ t)\end{bmatrix}^{\rm T}. \tag{9}$$

Finally, define $\Delta u(t) \triangleq \begin{bmatrix}\delta u_1(t) & \delta u_2(t) & \cdots & \delta u_m(t)\end{bmatrix}^{\rm T}$ given by the expression

$$\Delta u(t) = K_{\rm esc} \int_0^t \tilde{\mathcal{J}}_u\ dt. \tag{10}$$

Note that although different $K_{\rm esc}$ can be chosen for each component of $\tilde{\mathcal{J}}_u$, in the proposed scheme only one is considered, as shown in (10). Thus, a, $K_{\rm esc}$ and $\begin{bmatrix}\omega_1 & \omega_2 & \cdots & \omega_m\end{bmatrix}$ are the tuning parameters.

IV. Overview of Retrospective Cost based Extremum Seeking Control

An overview of the RC/ESC algorithm is presented in this section. Subsections IV-A and IV-B provide a brief review of RCAC and its specialization to adaptive PID control, respectively. Subsection IV-C describes an online gradient estimator based on the KF [1] . Subsection IV-D expands RCAC presented in Subsection IV-A to include gradient estimates obtained via the technique presented in Subsection IV-C, resulting in RC/ESC.

A. Review of Retrospective Cost Adaptive Control

RCAC is described in detail in [18]. Consider the strictly proper, discrete-time, input-output controller

$$\delta u_k = \sum_{i=1}^{l_{\rm c}} P_{i,k} u_{k-i} + \sum_{i=1}^{l_{\rm c}} Q_{i,k} z_{k-i}, \tag{11}$$

where $k \geq 0$ is the time step, $\delta u_k \in \mathbb{R}^{l_{\rm u}}$ is the controller output and thus the control input, $u_k \in \mathbb{R}^{l_{\rm u}}$ is the applied control input, $z_k \in \mathbb{R}^{l_{\rm z}}$ is the measured performance variable, $l_{\rm c}$ is the controller-window length, and, for all $i \in \{1, \ldots, l_{\rm c}\}$, $P_{i,k} \in \mathbb{R}^{l_{\rm u}\times l_{\rm u}}$ and $Q_{i,k} \in \mathbb{R}^{l_{\rm u}\times l_{\rm z}}$ are the controller coefficient matrices. In particular, u_k results from

[1] Subsections IV-A, IV-B and IV-C are described in more detail in https://arxiv.org/abs/2402.03717.

adding a vanishing perturbation signal to δu_k, as defined in Subsection IV-D. The controller shown in (11) can be written as

$$u_k = \phi_k \theta_k, \tag{12}$$

where

$$\phi_k \triangleq [\, u_{\mathrm{c},k-1}^{\mathsf{T}} \ \cdots \ u_{\mathrm{c},k-l_\mathrm{c}}^{\mathsf{T}} \ z_{k-1}^{\mathsf{T}} \ \cdots \ z_{k-l_\mathrm{c}}^{\mathsf{T}} \,] \otimes I_{l_\mathrm{u}} \in \mathbb{R}^{l_\mathrm{u} \times l_\theta}, \tag{13}$$

$$\theta_k \triangleq \mathrm{vec}\,[\, P_{1,k} \cdots P_{l_\mathrm{c},k} \ Q_{1,k} \cdots Q_{l_\mathrm{c},k} \,] \in \mathbb{R}^{l_\theta}, \tag{14}$$

$l_\theta \triangleq l_\mathrm{c} l_\mathrm{u}(l_\mathrm{u} + l_\mathrm{z})$, θ_k is the vector of controller coefficients, which are updated at each time step k, and $\otimes$ is the Kroenecker product.

Next, define the retrospective cost variable

$$\hat{z}_k(\hat{\theta}) = z_k - N_k(U_k - \Phi_k \hat{\theta}), \tag{15}$$

where $\hat{z}_k$ is the retrospective-cost variable, $\hat{\theta} \in \mathbb{R}^{l_\theta}$ is the controller coefficient vector determined by retrospective-cost optimization,

$$\Phi_k \triangleq \begin{bmatrix} \phi_{k-1}^{\mathsf{T}} & \ldots & \phi_{k-l_\mathrm{f}}^{\mathsf{T}} \end{bmatrix}^{\mathsf{T}} \in \mathbb{R}^{l_\mathrm{f} l_\mathrm{u} \times l_\theta}, \tag{16}$$

$$U_k \triangleq \begin{bmatrix} \delta u_{k-1} & \ldots & \delta u_{k-l_\mathrm{f}} \end{bmatrix}^{\mathsf{T}} \in \mathbb{R}^{l_\mathrm{f} l_\mathrm{u}}, \tag{17}$$

$$N_k \triangleq [\, N_{1,k} \ \cdots \ N_{l_\mathrm{f},k} \,] \in \mathbb{R}^{l_\mathrm{z} \times l_\mathrm{f} l_\mathrm{u}}. \tag{18}$$

For the present work, N_k is updated online and is used to determine a direction based on the estimated gradient of the performance variable z_k. The algorithm used to determine N_k at each step k is given in Subsection IV-D.

The controller gain θ_k is updated by the retrospective cost optimization, as described in detail in Subsection 3.1 in [22]. This update procedure requires the choice of certain hyperparameters, which include an initial convariance, positive definite matrix $P_0 \in \mathbb{R}^{l_\theta \times l_\theta}$, and a control input weighting, positive semidefinite matrix $R_\mathrm{u} \in \mathbb{R}^{l_\mathrm{u} \times l_\mathrm{u}}$. For all of the numerical simulations and physical experiments in this work, θ_k is initialized as $\theta_0 = 0_{l_\theta \times 1}$ to reflect the absence of additional prior modeling information. The matrices P_0 and R_u have the form $P_0 = p_0 I_{l_\theta}$ and $R_\mathrm{u} = r_\mathrm{u} I_m$, where the positive scalar p_0 and nonnegative scalar r_u determine the rate of adaptation.

B. RCAC-based PID

Let δu_k be given by

$$\delta u_k = \kappa_{\mathrm{p},k} z_{k-1} + \kappa_{\mathrm{i},k} \zeta_{k-1} + \kappa_{\mathrm{d},k}(z_{k-1} - z_{k-2}), \tag{19}$$

where $\kappa_{\mathrm{p},k}$, $\kappa_{\mathrm{i},k}$, and $\kappa_{\mathrm{d},k}$ are time-varying PID gains and ζ_k is given by the integrator $\zeta_k \triangleq \sum_{j=0}^{k} z_j$. The control (19) can be expressed as (12), where

$$\phi_k \triangleq \begin{bmatrix} z_{k-1} & \zeta_{k-1} & z_{k-1} - z_{k-2} \end{bmatrix} \in \mathbb{R}^{1 \times 3}, \tag{20}$$

$$\theta_k \triangleq \begin{bmatrix} \kappa_{\mathrm{p},k} & \kappa_{\mathrm{i},k} & \kappa_{\mathrm{d},k} \end{bmatrix}^{\mathsf{T}} \in \mathbb{R}^3. \tag{21}$$

Note that the regressor ϕ_k is constructed from the past values of z_k and ζ_k, and the controller coefficient vector θ_k contains the time-dependent proportional, integral, and derivative gains $\kappa_{\mathrm{p},k}$, $\kappa_{\mathrm{i},k}$, and $\kappa_{\mathrm{d},k}$. Furthermore, note that the adaptive digital PID control can be specialized to adaptive digital PI, PD, ID, P, I, and D control by omitting the corresponding components of ϕ_k and θ_k. Then, RCAC-based PID (RCAC/PID) is (12) with (20) and (21), respectively.

C. Online gradient estimator using a Kalman Filter

For all $k \geq 0$, let $J_k \triangleq [J_{1,k} \ \ \cdots \ \ J_{l_J,k}]^{\mathsf{T}} \in \mathbb{R}^{l_J}$ be a cost function vector computed from system measurements, where, for all $i \in \{1, \ldots, l_J\}$, $J_{i,k} \geq 0$ is the ith component of J_k, let u_k be the control input, and let $\nabla J_k \triangleq [\nabla J_{1,k} \ \ \cdots \ \ \nabla J_{l_J,k}]^{\mathsf{T}} \in \mathbb{R}^{l_J \times m}$ be the gradient of J_k over u_k, where, for all $i \in \{1, \ldots, l_J\}$, the transpose of $\nabla J_{i,k} \in \mathbb{R}^m$ corresponds to the ith row of ∇J_k.

Next, let $i \in \{1, \ldots, l_J\}$. Consider the measurement model for $J_{i,k}$

$$J_{i,k} = J_{\mathrm{b},i} + \nabla J_{i,k}^{\mathsf{T}} u_k, \tag{22}$$

where $J_{\mathrm{b},i} \in \mathbb{R}$ is a bias variable. Note that (22) is an extension of (17) from [25]. Furthermore, let $\nabla \hat{J}_{i,k} \in \mathbb{R}^m$ be an estimate of $\nabla J_{i,k}$, let $\hat{J}_{\mathrm{b},i} \in \mathbb{R}$ be an estimate of $J_{\mathrm{b},i}$, let $\hat{x}_{i,k} \triangleq \begin{bmatrix} \nabla \hat{J}_{i,k}^{\mathsf{T}} & \hat{J}_{\mathrm{b},i} \end{bmatrix}^{\mathsf{T}} \in \mathbb{R}^{m+1}$ be an estimate of $x_{i,k} \triangleq \begin{bmatrix} \nabla J_{i,k}^{\mathsf{T}} & J_{\mathrm{b},i} \end{bmatrix}^{\mathsf{T}}$, and let $P_{i,k} \in \mathbb{R}^{(m+1)\times(m+1)}$ be the covariance of the estimate $\hat{x}_{i,k}$ of $x_{i,k}$. Then, as indicated by (22) and Section 3.1 of [25], the estimate $\nabla \hat{J}_{i,k}$ can be obtained using a KF with state and measurement equations given by

$$x_{i,k+1} = x_{i,k} + w_{i,k}, \tag{23}$$

$$y_{i,k} \triangleq \begin{bmatrix} J_{i,k} \\ J_{i,k-k_1} \\ \vdots \\ J_{i,k-k_m} \end{bmatrix} = \begin{bmatrix} u_{k-1}^{\mathsf{T}} & 1 \\ u_{k-1-k_1}^{\mathsf{T}} & 1 \\ \vdots & \vdots \\ u_{k-1-k_m}^{\mathsf{T}} & 1 \end{bmatrix} x_{i,k} + v_{i,k}, \tag{24}$$

where $y_{i,k} \in \mathbb{R}^{m+1}$ is the measurement vector and $w_{i,k}, v_{i,k} \in \mathbb{R}^{m+1}$ are Gaussian random variables. Hence, it follows from (23), (24) that the estimate $\nabla \hat{J}_{i,k}$ is given by the recursive update of the KF, whose prediction and update equations are given, for $i \in \{1, \ldots, l_J\}$, by

$$\hat{x}_{i,k} = \hat{x}_{i,k-1} + K_{i,k-1}\left(G_{i,k-1} - H_{k-1}\hat{x}_{i,k-1}\right), \tag{25}$$

$$P_{i,k} = (I_{m+1} - K_{i,k-1}H_{k-1})(P_{i,k-1} + Q_i), \tag{26}$$

$$\nabla \hat{J}_{i,k} = [I_m \ \ 0_{m\times 1}]\, \hat{x}_{i,k}, \tag{27}$$

where

$$G_{i,k-1} \triangleq \begin{bmatrix} J_{i,k-1} \\ J_{i,k-1-k_1} \\ \vdots \\ J_{i,k-1-k_m} \end{bmatrix} \in \mathbb{R}^{m+1}, \ H_{k-1} \triangleq \begin{bmatrix} u_{k-1}^{\mathsf{T}} & 1 \\ u_{k-1-k_1}^{\mathsf{T}} & 1 \\ \vdots & \vdots \\ u_{k-1-k_m}^{\mathsf{T}} & 1 \end{bmatrix} \in \mathbb{R}^{(m+1)\times(m+1)},$$

$$K_{i,k-1} \triangleq [(P_{i,k-1} + Q_i)H_{k-1}^{\mathsf{T}}][H_{k-1}(P_{i,k-1} + Q_i)H_{k-1}^{\mathsf{T}} + R_i]^{-1} \in \mathbb{R}^{(m+1)\times(m+1)},$$

$Q_i, R_i \in \mathbb{R}^{(m+1)\times(m+1)}$ are the constant weighting matrices, and $0 < k_1 < \cdots < k_m$ are indices. The matrices Q_i and R_i determine the rate of estimation, and $k_1, \ldots, k_m$ are chosen to enhance the accuracy of the estimate $\hat{x}_{i,k}$. Finally, the estimate $\nabla \hat{J}_k$ is given by

$$\nabla \hat{J}_k \triangleq \begin{bmatrix} \nabla \hat{J}_{1,k} & \cdots & \nabla \hat{J}_{l_J,k} \end{bmatrix}^{\mathsf{T}} \in \mathbb{R}^{l_J \times m}. \tag{28}$$

For all of the numerical simulations in the present work, $\hat{x}_{i,k}$ is initialized as $\hat{x}_{i,0} = 0_{m\times 1}$. The matrices $P_{i,0}$, Q_i, and R_i have the form $P_{i,0} = p_{i,0} I_{m+1}$, $Q_i = q_i I_{m+1}$, and $R_i = r_i I_{m+1}$, where the positive scalars $p_{i,0}$, q_i, and r_i determine the rate of estimation.

D. Retrospective Cost based Extremum Seeking Control

As shown in Figure 3, RC/ESC includes RCAC described in Subsection IV-A, the KF gradient estimator described in Subsection IV-C, a normalization function, and a gradient conversion function. For RC/ESC, $l_J = p$ and $l_{\rm f} = m$. RC/ESC operates on the cost-function vector $J_k \in \mathbb{R}^p$ and $u_{k-1} \in \mathbb{R}^m$ to produce the RC/ESC output vector $u_k \in \mathbb{R}^m$. As mentioned in subsection IV-C, for all $i \in \{1, \ldots, p\}$, $J_{i,k} > 0$. The objective of RC/ESC is to minimize the components of J_k by modulating u_k, that is,

$$\min_{(u_n)_{n=0}^{\infty}} \ \limsup_{k\to\infty} \sum_{i=1}^{p} J_{i,k}. \tag{29}$$

The performance variable z_k used by RCAC is obtained by normalizing J_k using

$$z_k \overset{\triangle}{=} [I_p + \nu \ \mathrm{diag}\,(J_k)]^{-1} J_k, \tag{30}$$

where $\nu \in [0, \infty)$. Next, the gradient estimator block operates on J_k and u_k to produce $\nabla \hat{J}_{k+1}$ by using the KF-based estimator described in Subsection IV-C. The gradient conversion block yields $N_k = [N_{1,k} \ \ \cdots \ \ N_{m,k}]$, such that, for all $i \in \{1, \ldots, m\}$,

$$N_{i,k} = \begin{bmatrix} & \overline{\nabla} \hat{J}_{1,i,k+1} & \\ 0_{p\times(i-1)} & \vdots & 0_{p\times(m-i)} \\ & \overline{\nabla} \hat{J}_{p,i,k+1} & \end{bmatrix}, \tag{31}$$

where, for all $j \in \{1, \ldots, p\}$,

$$\overline{\nabla} \hat{J}_{j,i,k+1} \overset{\triangle}{=} \begin{cases} \nabla \hat{J}_{j,i,k+1} / \left|\left|\nabla \hat{J}_{j,k+1}\right|\right|, & \left|\left|\nabla \hat{J}_{j,k+1}\right|\right| \geq \varepsilon \\ \nabla \hat{J}_{j,i,k+1} / \varepsilon, & \text{otherwise}, \end{cases} \tag{32}$$

$\nabla \hat{J}_{j,i,k+1}$ is the ith component of $\nabla \hat{J}_{j,k+1}$, and $\varepsilon > 0$. We fix $\varepsilon = 10^{-4}$ throughout the present work. The RCAC block then uses z_k, N_k, and u_{k-1} to produce $\delta u_k \in \mathbb{R}^m$ by using the operations described in Subsection IV-A.

Finally, define $u_k \overset{\triangle}{=} \delta u_k + d_k$, where $d_k \in \mathbb{R}^m$ is a vanishing perturbation signal. Note that, while [25] uses only $\nabla \hat{J}_{k+1}$, RC/ESC uses J_k and $\nabla \hat{J}_{k+1}$ in the form of z_k and N_k, respectively.

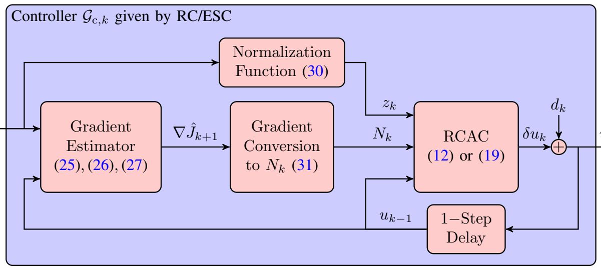
Controller $\mathcal{G}_{{\rm c},k}$ given by RC/ESC
J_k
Normalization Function (30)
Gradient Estimator (25), (26), (27)
$\nabla \hat{J}_{k+1}$
Gradient Conversion to N_k (31)
z_k
N_k
RCAC (12) or (19)
δu_k
d_k
u_k
u_{k-1}
1−Step Delay

Fig. 3: RC/ESC block diagram.

V. Numerical Examples

In this section, RC/ESC is implemented in numerical simulations to illustrate its performance and compare it with the continuous-time ESC algorithms presented in Section III. Example 5.1 features a static optimization problem in a SISO system. Example 5.2 features a static optimization problem in a MISO system. Example 5.3 features a dynamic optimization problem in a SISO system. In Examples 5.1 and 5.2, $T_{\rm s} = 1$ s. In Example 5.3, $T_{\rm s} = 5$ s. Tables I and II show the RC/ESC and ESC hyperparameters, respectively, used in the numerical examples. Note that in Example 5.1 a RCAC/I controller is implemented, that is an RCAC-based integrator controller, as mentioned in Subsection IV-B. Examples 5.2 and 5.3 implement the general case RCAC introduced in Subsection IV-A.

TABLE I: RC/ESC hyperparameters in numerical examples

	RCAC				KF					
Example	**Type**	$l_{\rm c}$	$r_{\rm u}$	p_0	$p_{1,0}, p_{2,0}$	q_1, q_2	r_1, r_2	k_1	k_2	ν
5.1	RCAC/I	-	0.05	0.9	10^{-3}	0.1	10	3	-	0.9
5.2	RCAC	5		0.1	10^{-4}		0.1	2	6	0.2
5.3			0.01			0.01	1			

TABLE II: ESC hyperparameters in numerical examples

Example	a	$K_{\rm esc}$	ω_1	ω_2
5.1	0.2	0.05	6	-
5.2	0.3		30	50
5.3	0.2	5	3	5

Example 5.1: Static optimization in SISO system. Consider the static system

$$J(t) = (u(t) - r(t))^2 \tag{33}$$

where $u \in \mathbb{R}$, for $t \in [0, 500]$, $r(t) = 1$, and for $t > 500$, $r(t) = 5$. As mentioned in Section II, the objective is to minimize J. Furthermore, the dither signals are shown in 6. The results of the numerical simulations are shown in Figures 4 and 5. While the response of RC/ESC converges to the minimizer in a slow manner, note that the response of RC/ESC does not oscillate around the minimizer since the dither is close to zero throughout the operation and eventually vanishes. ◇

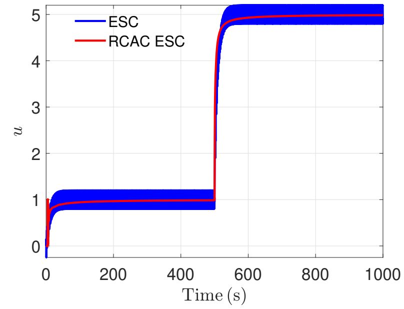

Fig. 4: Example 5.1: **SISO Static map**. Controller output u for the static map given by (33) with ESC and RC/ESC. Note that the ESC response is shown in blue and the RC/ESC response is shown in red.

Example 5.2: Static optimization in MISO system. Consider the static system

$$J(t) = (u(t) - r(t))^{\mathsf{T}}(u(t) - r(t)) \tag{34}$$

where, $u \overset{\triangle}{=} [u_1 \ \ u_2]^{\mathsf{T}} \in \mathbb{R}^2$, for $t \in [0, 500]$, $r(t) = [1 \ \ 2]^{\mathsf{T}}$, and for $t > 500$, $r(t) = [-1 \ \ -2]^{\mathsf{T}}$. As mentioned in Section II, the objective is to minimize J. Furthermore, the dither signals are shown in 9. The results of the numerical simulations are shown in Figures 7 and 8. While the response of RC/ESC converges to the minimizer in a slow manner, note that the response of RC/ESC does not

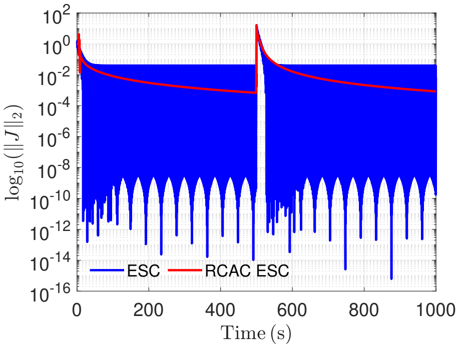

Fig. 5: Example 5.1: **SISO Static map**. Output error with respect to the optimal value $J = 0$ in log scale with ESC and RC/ESC. Note that the error by ESC is shown in blue and the error by RC/ESC is shown in red.

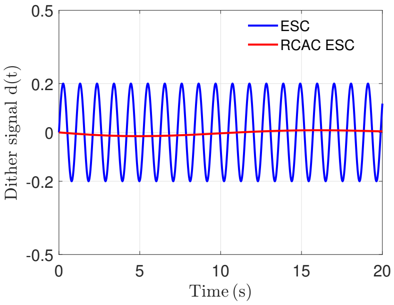

Fig. 6: Example 5.1: **SISO Static map**. Dither signal with ESC and RC/ESC. Note that the ESC dither signal is shown in blue and the RC/ESC dither signal is shown in red.

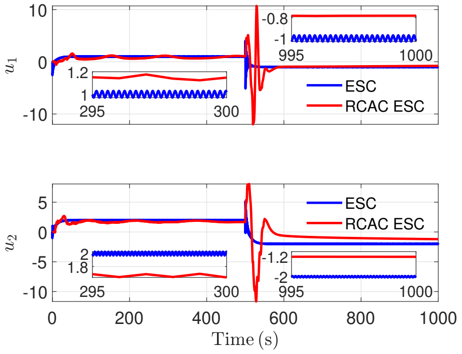

Fig. 7: Example 5.2: **MISO Static map**. Controller output components $u_{(1)}$ and $u_{(2)}$ for the static map given by (34) with ESC and RC/ESC. Note that the ESC response is shown in blue and the RC/ESC response is shown in red.

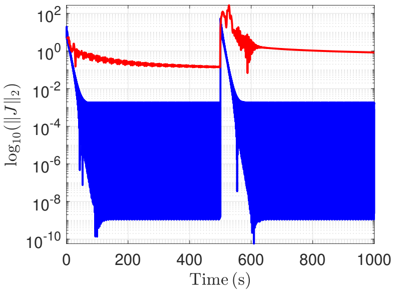

Fig. 8: Example 5.2: **MISO Static map**. Output error with respect to the optimal value $J = 0$ in log scale with ESC and RC/ESC. Note that the error by ESC is shown in blue and the error by RC/ESC is shown in red.

oscillate around the minimizer since the dither quickly goes to zero throughout the operation and eventually vanishes. ◇

Example 5.3: Dynamic optimization in MISO system (control gain tuning for stabilization).

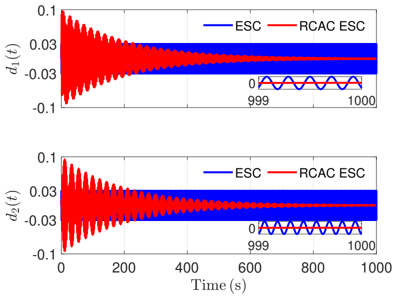

Fig. 9: Example 5.2: **MISO Static map**. Dither signals with ESC and RC/ESC. Note that the ESC dither signals are shown in blue and the RC/ESC dither signals are shown in red.

Consider the Van Der Pol system

$$\ddot{x} + x + (\dot{x}^2 - 1)\dot{x} = u, \tag{35}$$

where $x_1 = x$ and $x_2 = \dot{x}$. Also, consider the full-state feedback controller structure given by

$$u = \begin{bmatrix} K_1 & K_2 \end{bmatrix} \begin{bmatrix} x_1 \\ x_2 \end{bmatrix}. \tag{36}$$

Also, an amplitude detector scheme is considered using moving standard deviation for each state and adding them along the entire horizon. Thus, the cost function J is the amplitude of the oscillations of the states and ESC and RCAC-ESC are used to find suitable values of $\begin{bmatrix} K_1 & K_2 \end{bmatrix}$ in such a way that $J = 0$ and thus, the system could be asymptotically stabilized. As mentioned in Section II, the objective is to minimize J. Furthermore, the dither signals are shown in 13. The results of the numerical simulations are shown in Figures 10, 11 and 12. Both ESC and RC/ESC yield values of K_1 and K_2 that stabilize the response of the Van Der Pol system While the response of RC/ESC converges to the minimizer in a slow manner, note that the response of RC/ESC does not oscillate around the minimizer since the dither quickly goes to zero throughout the operation and eventually vanishes. ◇

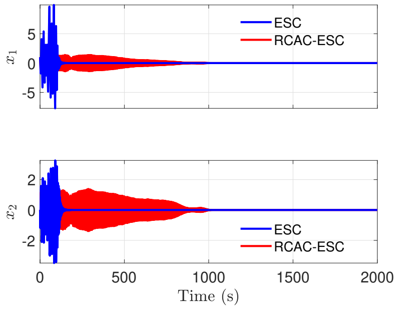

Fig. 10: Example 5.3: **MISO Dynamic map**. Components of the Van Der Pol system state x versus time with ESC and RC/ESC. Note that the ESC result is shown in blue and the RC/ESC result is shown in red.

VI. Conclusions

This paper introduced a retrospective cost-based ESC controller for online output minimization with a vanishing perturbation. A KF is used to estimate the gradient of the system output at each step, which is then used to construct a target model that provides RCAC with a search direction to obtain a control input that minimizes the system output. Numerical examples illustrate the performance of this technique

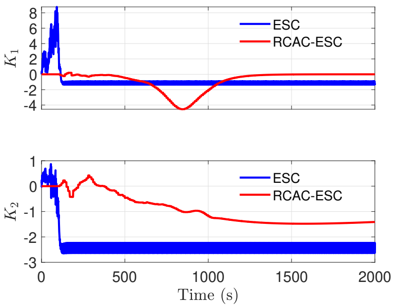

Fig. 11: Example 5.3: **MISO Dynamic map**. Controller gains K_1 and K_2 versus time with ESC and RC/ESC. Note that the ESC response is shown in blue and the RC/ESC response is shown in red.

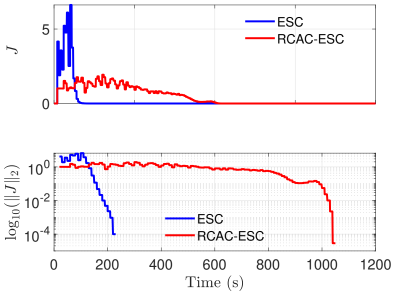

Fig. 12: Example 5.3: **MISO Dynamic map**. Output error with respect to the optimal value $J = 0$ in regular and log scale with ESC and RC/ESC. Note that the error by ESC is shown in blue and the error by RC/ESC is shown in red.

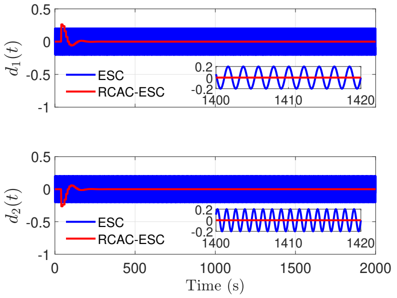

Fig. 13: Example 5.3: **MISO Dynamic map**. Dither signals with ESC and RC/ESC. Note that the ESC dither signals are shown in blue and the RC/ESC dither signals are shown in red.

and provide a comparison with a regular continuous-time ESC scheme. Future work will focus on modifications for faster convergence and implementation in physical systems with time-varying minimizers.

References

[1] K. B. Ariyur and M. Krstić, *Real-Time Optimization by Extremum-Seeking Control*. John Wiley & Sons, 2003.

[2] M. Krstić, “Performance improvement and limitations in extremum seeking control,” *Systems & Control Letters*, vol. 39, no. 5, pp. 313–326, 2000.

[3] M. Krstić and H.-H. Wang, “Stability of extremum seeking feedback for general nonlinear dynamic systems,” *Automatica*, vol. 36, no. 4, pp. 595–601, 2000.

[4] Y. Tan, W. H. Moase, C. Manzie, D. Nešić, and I. M. Mareels, “Extremum seeking from 1922 to 2010,” in *Proc. Chin. Contr. Conf.* IEEE, 2010, pp. 14–26.

[5] A. S. Matveev, M. C. Hoy, and A. V. Savkin, “Extremum seeking navigation without derivative estimation of a mobile robot in a dynamic environmental field,” *IEEE Trans. Contr. Syst. Tech.*, vol. 24, no. 3, pp. 1084–1091, 2015.

[6] M. Bagheri, M. Krstić, and P. Naseradinmousavi, “Multivariable extremum seeking for joint-space trajectory optimization of a high-degrees-of-freedom robot,” *J. Dyn. Syst. Meas. Contr.*, vol. 140, no. 11, p. 111017, 2018.

[7] B. Calli, W. Caarls, M. Wisse, and P. P. Jonker, “Active vision via extremum seeking for robots in unstructured environments: Applications in object recognition and manipulation,” *IEEE Trans. Automat. Sci. Eng.*, vol. 15, no. 4, pp. 1810–1822, 2018.

[8] F. E. Sotiropoulos and H. H. Asada, “A model-free extremum-seeking approach to autonomous excavator control based on output power maximization,” *IEEE Robot. Automat. Lett.*, vol. 4, no. 2, pp. 1005–1012, 2019.

[9] A. Ghaffari, M. Krstić, and S. Seshagiri, “Power optimization and control in wind energy conversion systems using extremum seeking,” *IEEE Trans. Contr. Syst. Tech.*, vol. 22, no. 5, pp. 1684–1695, 2014.

[10] M. Ye and G. Hu, “Distributed extremum seeking for constrained networked optimization and its application to energy consumption control in smart grid,” *IEEE Trans. Contr. Syst. Tech.*, vol. 24, no. 6, pp. 2048–2058, 2016.

[11] N. Bizon, “Energy optimization of fuel cell system by using global extremum seeking algorithm,” *Appl. Energy*, vol. 206, pp. 458–474, 2017.

[12] D. Zhou, A. Al-Durra, I. Matraji, A. Ravey, and F. Gao, “Online energy management strategy of fuel cell hybrid electric vehicles: A fractional-order extremum seeking method,” *IEEE Trans. Indust. Electr.*, vol. 65, no. 8, pp. 6787–6799, 2018.

[13] L. Wang, S. Chen, and K. Ma, “On stability and application of extremum seeking control without steady-state oscillation,” *Automatica*, vol. 68, pp. 18–26, 2016.

[14] M. Haring and T. A. Johansen, “Asymptotic stability of perturbation-based extremum-seeking control for nonlinear plants,” *IEEE Trans. Autom. Contr.*, vol. 62, no. 5, pp. 2302–2317, 2016.

[15] ——, “On the accuracy of gradient estimation in extremum-seeking control using small perturbations,” *Automatica*, vol. 95, pp. 23–32, 2018.

[16] C. Yin, S. Dadras, X. Huang, Y. Chen, and S. Zhong, “Optimizing energy consumption for lighting control system via multivariate extremum seeking control with diminishing dither signal,” *Trans. Automat. Sci. Eng.*, vol. 16, no. 4, pp. 1848–1859, 2019.

[17] D. Bhattacharjee and K. Subbarao, “Extremum seeking control with attenuated steady-state oscillations,” *Automatica*, vol. 125, p. 109432, 2021.

[18] Y. Rahman, A. Xie, and D. S. Bernstein, “Retrospective Cost Adaptive Control: Pole Placement, Frequency Response, and Connections with LQG Control,” *IEEE Contr. Sys. Mag.*, vol. 37, pp. 28–69, Oct. 2017.

[19] A. Goel and D. S. Bernstein, “Gradient-, Ensemble-, and Adjoint-Free Data-Driven Parameter Estimation,” *J. Guid. Contr. Dyn.*, vol. 42, no. 8, pp. 1743–1754, 2019.

[20] ——, “Retrospective cost parameter estimation with application to space weather modeling,” *Handbook of Dynamic Data Driven Applications Systems: Volume 2*, pp. 603–625, 2023.

[21] J. Paredes, R. Ramesh, S. Obidov, M. Gamba, and D. Bernstein, “Experimental investigation of adaptive feedback control on a dual-swirl-stabilized gas turbine model combustor,” in *AIAA Prop. Energy Forum*, 2022, p. 2058.

[22] J. A. Paredes, R. Ramesh, M. Gamba, and D. S. Bernstein, “Experimental application of a quasi-static adaptive controller to a dual independent swirl combustor,” *Combustion Science and Technology*, pp. 1–34, 2024, dOI: 10.1080/00102202.2024.2306301.

[23] D. Nešić, “Extremum seeking control: Convergence analysis,” *European Journal of Control*, vol. 15, no. 3-4, pp. 331–347, 2009.

[24] K. B. Ariyur and M. Krstic, *Real-time optimization by extremum-seeking control*. John Wiley & Sons, 2003.

[25] G. Gelbert, J. P. Moeck, C. O. Paschereit, and R. King, “Advanced algorithms for gradient estimation in one-and two-parameter extremum seeking controllers,” *J. Proc. Contr.*, vol. 22, no. 4, pp. 700–709, 2012.